Channel-Containing Criss-Crossed and Hydrogen-Bonded One-Dimensional Coordination Polymers of Iron(III) and (II) with 4,4′-Bipyridine: Hydrothermal Syntheses, Structures, Absorption and Mössbauer Studies Showing Spin Crossover for the Iron(III) Polymer

Khalid Abu-Shandi[a], Heiner Winkler[b], Hauke Paulsen[b], Robert Glaum[c], Biao Wu[a], and Christoph Janiak[a,*]

[a] Freiburg, Institut für Anorganische und Analytische Chemie
[b] Universität zu Lübeck, Institut für Physik, Ratzeburger Allee 160, D-23538 Lübeck
[c] Universität Bonn, Institut für Anorganische Chemie, Gerhard-Domagk-Str. 1, D-53121 Bonn

Received March 9th, 2005.

Dedicated to Professor Herbert W. Roesky on the Occasion of his 70th Birthday

Abstract. The iron-4,4′-bipyridine coordination polymers $^{1}_{\infty}${[Fe^{III}(NO_3)$_2$(μ-4,4′-bipy)(H_2O)$_2$]OH·H_2O} (**1**) and $^{1}_{\infty}${[Fe^{II}(H_2PO_4)$_2$-(μ-4,4′-bipy)(H_2O)]·H_2O·(4,4′-bipy)} (**2**) have been synthesized by hydrothermal methods. The structure of **1** is a channel-containing open framework constructed through the hydrogen-bond supported criss-cross arrangement of the 1D Fe-bipy chains. ^{57}Fe Mössbauer spectroscopy reveals a gradual spin crossover behavior for **1** with a magnetic ordering at low temperature. The structure of **2** is constructed from parallel oriented, hydrogen-bonded 1D Fe-bipy chains. The 4,4′-bipyridine solvate in **2** is held by hydrogen bonding between the H_2PO_4 groups on adjacent iron centers along the chain and is situated in a π−π stacking contact to the coordinated 4,4′-bipy ligand. The chains in **2** are interconnected through hydrogen bonding to a three-dimensional supramolecular network. Crystals of **2** appear dark red or orange depending on the orientation (pleochroism, dichroism).

Keywords: Coordination polymers; Bipyridine; Iron; Mössbauer; Pleochroism

Introduction

The compound 4,4′-bipyridine (4,4′-bipy) is a prominent example for a prototypical bridging ligand and an attractive molecular building block for diverse architectures of coordination polymers (metal-organic coordination networks) [1−5] such as one-dimensional (1D) chains [6] or ladders [7], two-dimensional (2D) grids [8−13] and three-dimensional frameworks [14−16]. 4,4′-Bipyridine cannot only function as a linear spacer between metal connectors but also as a hydrogen-bond acceptor [17]. Several metal-organic coordination networks with two types of 4,4′-bipy bridging ligands − metal coordinating (**A**) and hydrogen-bonding (**B**) − have been reported [2, 18−21, see also the following Fe-bipy examples]. Coordination polymers with extended iron-4,4′-bipy substructures, which are of interest for comparison to the structures reported here, include $^{1}_{\infty}${[Fe^{II}(ClO_4)$_2$(μ-4,4′-bipy)(H_2O)$_2$]·(4,4′-bipy)} and $^{1}_{\infty}${[Fe^{II}(ClO_4)(μ-4,4′-bipy)(H_2O)$_3$]ClO_4·H_2O·1.5(4,4′-bipy)} [21], $^{1}_{\infty}${[Fe^{II}(NCS/Se)$_2$(μ-4,4′-bipy)(H_2O)$_2$]·4,4′-bipy} (S: [22], S, Se: [23]), $^{1}_{\infty}${Fe^{II}(NCS)$_2$(μ-4,4′-bipy)(2,2′-bi(2-thiazoline))} [24], $^{1}_{\infty}${[Fe^{II}(μ-4,4′-bipy)(2-(pyrid-2-yl)imidazole)$_2$](ClO_4)$_2$·EtOH} [25], $^{1}_{\infty}${Fe^{II}($N(SiMe_3)_2$)$_2$(μ-4,4′-bipy)} [26], $^{1}_{\infty}${[Fe^{II}(dicyanamido)$_2$(μ-4,4′-bipy)(H_2O)$_2$]·(4,4′-bipy)} [27], $^{2}_{\infty}${Fe^{II}(μ-Cl)$_2$(μ-4,4′-bipy)} [28], $^{2}_{\infty}${Fe^{II}(μ-C_2O_4)(μ-4,4′-bipy)} [29], $^{2}_{\infty}${Fe^{II}_3(μ-C_2O_4)$_3$(μ-4,4′-bipy)$_2$(4,4′-bipy)$_2$} [30], $^{2}_{\infty}${[Fe^{II}_2(μ-C_{4O4})$_2$(μ-4,4′-bipy)$_2$]·3-6H_2O} [31], $^{2}_{\infty}${Fe^{II}(μ-CrO_4)(μ-4,4′-bipy)$_2$} [32], $^{3}_{\infty}${[4,4′-bipyH_2]-[Fe^{II}_3(μ-SO_4)$_4$(μ-4,4′-bipy)$_3$(H_2O)$_6$]·10H_2O} [33], $^{3}_{\infty}${Fe^{II}(μ-$^{N}_3$)$_2$-(μ-4,4′-bipy)} [34], $^{3}_{\infty}${Fe^{II}(μ-dicyanamido)$_2$(μ-4,4′-bipy)} (also as H_2O solvate) [27, 35] and molecular [Fe^{III}(NCS)$_3$(4,4′-bipy)$_2$]·acetone [36] and [Fe^{II}(4,4-bipy)$_2$-(H_2O)$_4$](saccharinat)$_2$·(4,4′-bipy)^2 [37]. The very recent nature of most of the aforementioned Fe-4,4′-bipy work, many of it in the realm of magnetism, shows the strong interest in Fe-4,4′-bipy compounds. The majority of the known Fe-4,4′-bipy structures contain Fe^{II}. Here, we describe the syntheses and structures of two polymeric iron-4,4′-bipyridine compounds, one of them with Fe^{III}, and investigate the electronic situation of the iron centers by ^{57}Fe Mössbauer spectroscopy.

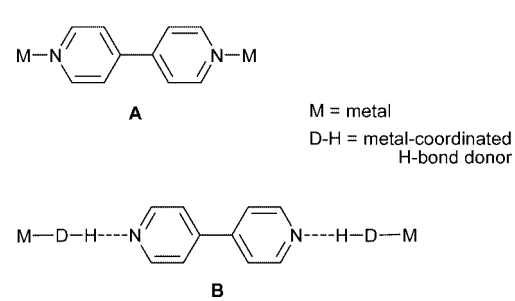

* Prof. Dr. Chr. Janiak
Institut für Anorganische und Analytische Chemie
Universität Freiburg
Albertstr. 21
D-79104 Freiburg
E-Mail: janiak@uni-freiburg.de

Results and Discussion

Compound $^{1}_{\infty}\{[Fe^{III}(NO_3)_2(\mu\text{-}4,4'\text{-bipy})(H_2O)_2]OH{\cdot}H_2O\}$ (1)

Hydrothermal treatment of 4,4′-bipyridine with iron(III) nitrate in the presence of tetra-*n*-butylammonium hydroxide in water at 165 °C yielded light-orange crystals which analyzed as the title compound (**1**) (eq. (1)) from Mössbauer and single-crystal X-ray diffraction.

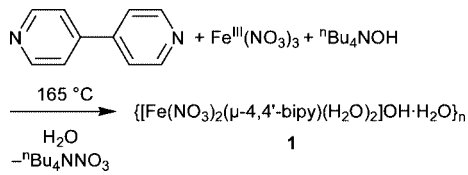

(1)

In the crystal structure (see below) the unligated oxygen atoms were highly disordered even at low temperature. Thus, their hydrogen atoms could not be found to enable an assignment as either two water molecules of crystallization (and Fe in oxidation state +II) or a hydroxide and one water of crystallization (and Fe in oxidation state +III). ^{57}Fe Mössbauer spectroscopy was used here to determine the iron oxidation state [38]. The Mössbauer spectra for compound **1** as a function of temperature, show two main features (Fig. 1, Table 1). First, at low temperature (4 K) there is a wide quadrupole doublet, while at room temperature this same wide doublet and a narrow doublet are observed. The narrow doublet is already visible at 77 K and grows in proportion with increasing temperature. As an explanation for these observations it can be assumed that at low temperature there is a low-spin Fe^{III} system for which a large quadrupole splitting from the unsymmetrical charge distribution would be expected. Furthermore, it must be assumed that the additional narrow doublet originates from a spin crossover equilibrium [39−41] which at higher temperatures favors high-spin Fe^{III} for which the observed isomer shift ($\delta^{\alpha-Fe} < 0.6$ mm s^{-1}) and small quadrupole splitting are then typical [42]. Otherwise, for high-spin Fe^{II} in an FeO_4N_2 coordination sphere an isomer shift around 1 mm s^{-1} and a quadrupole splitting above 2 mm s^{-1} would have had to be expected [30]. Mössbauer parameters obtained from density functional theory (DFT) calculations for Fe^{III} for *trans*-$[Fe(NO_3)_2(H_2O)_2(pyridine)_2]$ as a simple model for the iron environment in **1** (Table 2) show a fair agreement to the experimental values (cf. Table 1). Note that even though there is a symmetric charge distribution of high-spin d^5-Fe(III), there is a contribution for a small quadrupole splitting from the ligand field which is of lower than O_h symmetry (D_{4h} for a *trans*-FeO_4N_2 coordination and D_{2h} for a $FeO_2O'_2N_2$ coordination if the differences between the nitrato and the aqua ligands are taken into account) [43]. The well resolved resonance absorptions for both spin states indicate that the low-to high-spin relaxation rate must be slower than 10^7 s^{-1} [39]. The spin-transition is extremely gradual, starting below 77 K and is still incomplete at 293 K with 36 % of the iron atoms still in the low-spin state. The second feature is a magnetic sextet in the low-temperature spectrum at 4 K. The large magnetic field around 50 Tesla is consistent with Fe^{3+}. Thus, part of the Fe^{III} is magnetically ordered at low temperature. It is known that a very weak antiferromagnetic coupling can be transmitted through bridging 4,4′-bipy ligands [27, 28, 44, 45].

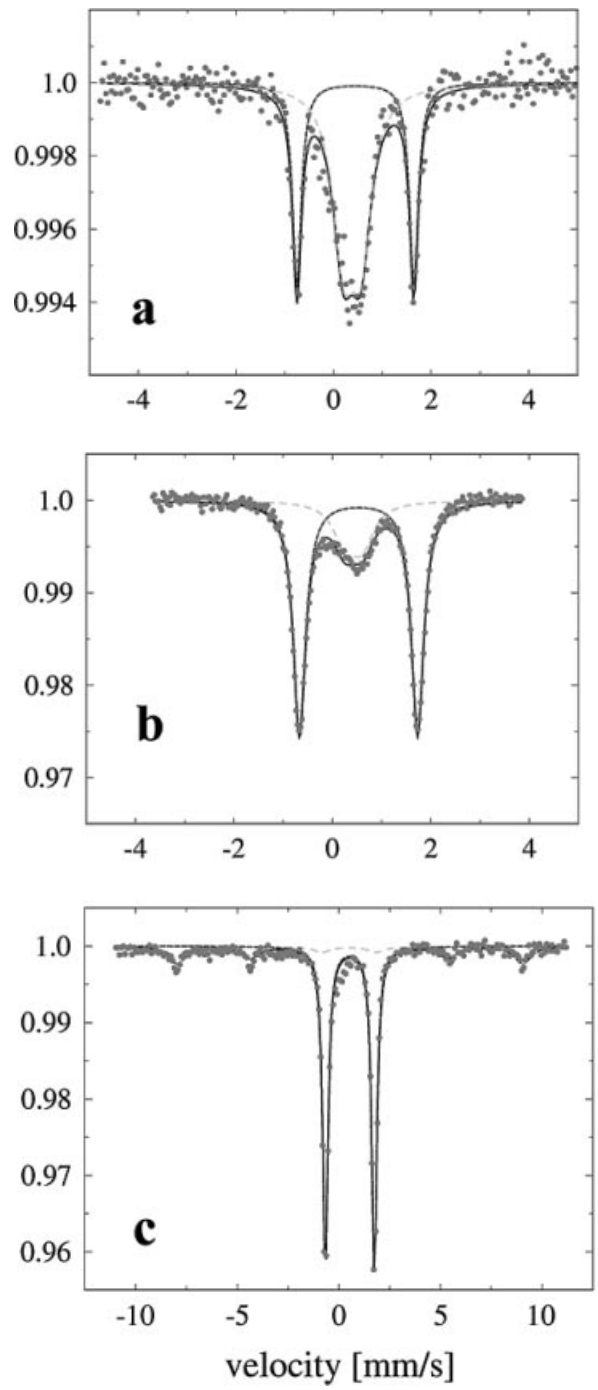

Fig. 1 Mössbauer spectra of $^{1}_{\infty}\{[Fe(NO_3)_2(\mu\text{-}4,4'\text{-bipy})(H_2O)_2]OH{\cdot}H_2O\}$ (**1**) at (a) room temperature, (b) T = 77 K and (c) T = 4.2 K. A sum of Lorentzians (solid lines) is used to fit the experimental data (dots); see Table 1 for individual parameters. The room temperature spectrum was also collected over the velocity range of ±10 mm s^{-1}, yet without the observation of any further signals.

Table 1 Mössbauer parameters for compound **1** [a]

Temp. K	Subspectrum	$\delta^{\alpha-Fe}$ [b] mm s^{-1}	ΔE_Q [c] mm s^{-1}	B_{hf} [d] Tesla	rel. area %
293	1 narrow doublet	0.38	0.36	–	64
(RT)	2 wide doublet	0.45	2.40	–	36
77	1 narrow doublet	0.44	0.35	–	24
	2 wide doublet	0.53	2.40	–	76
4.2	1 magnetic sextet	0.51	0.04	47.9	26
	2 wide doublet	0.53	2.21	–	74

[a] The errors of the hyperfine parameters are about 2 % and of the relative areas 5 %. [b] Isomer shift. [c] Quadrupole splitting. [d] Magnetic hyperfine field.

Table 2 Mössbauer parameters calculated with B3LYP/6-311G for *trans*-$[Fe(NO_3)_2(H_2O)_2(pyridine)_2]$ [a]

Oxid. state	Spin S	$\delta^{\alpha-Fe}$ [b] mm s^{-1}	ΔE_Q [c] mm s^{-1}
Fe^{II}	2 (high spin)	1.13	+3.53
	0 (low spin)	0.72	−1.04
Fe^{III}	5/2 (high spin)	0.48	+0.74
	1/2 (low spin)	0.32	−1.90

[a] Calculation based on the geometry optimized structure in each case. [b] Isomer shift. [c] Quadrupole splitting.

Thus, Mössbauer spectroscopy proved the Fe atoms to be in the nominal +3 oxidation state. Therefore, the formula for **1** was taken as $^1_\infty\{[Fe^{III}(NO_3)_2(\mu\text{-}4,4'\text{-bipy})(H_2O)_2]OH{\cdot}H_2O\}$. The crystal structure of **1** consists of Fe-bipy chains. Each iron atom is a center of symmetry and *trans*-coordinated by two nitrogen donors from bridging bipyridine groups, two nitrato and two aqua ligands (Fig. 2). Bond distances and angles between non-hydrogen atoms are listed in Table 3.

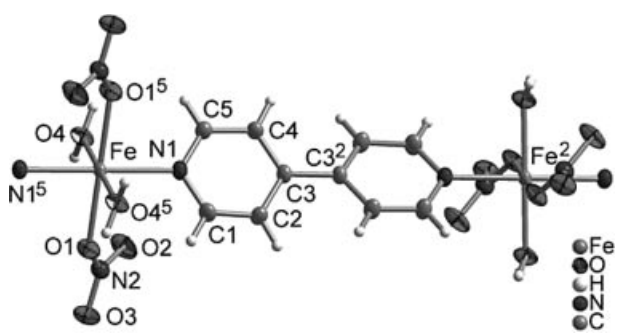

Fig. 2 Section of a single chain of $[Fe(NO_3)_2(\mu\text{-}4,4'\text{-bipy})(H_2O)_2]^+$ in **1**. Symmetry relations: 2 = 1.5−x, 1,5−y, z; 5 = 1−x, 1−y, −z.

Table 3 Selected bond lengths/Å and angles/° in **1**

Fe-O1	2.159(2)	O4-Fe-O1	81.12(6)
Fe-O4	2.060(2)	O4-Fe-N1	88.08(7)
Fe-N1	2.145(2)	N1-Fe-O1	94.33(7)

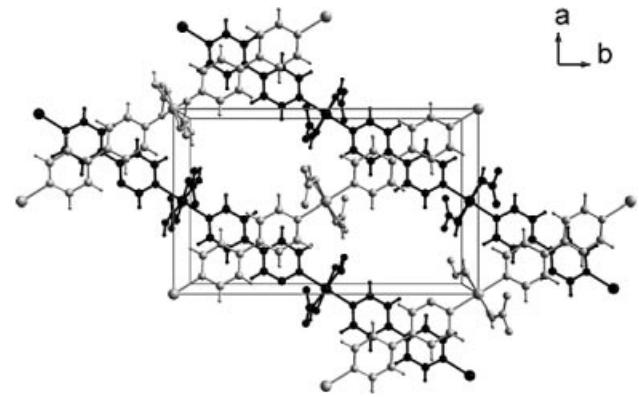

Fig. 3 Criss-cross packing of chains from adjacent layers (differentiated by grey or black) in **1** showing the formation of channels running along the *c*-direction and the π−π stacking between bipyridine ligands from adjacent layers.

Parallel chains are arranged in layers perpendicular to the *c* axis within the (001)- and the (002)-plane. Chains from adjacent layers run in different directions to give a criss-cross pattern (Fig. 3). Chains from the (001)-plane run colinear with the (1-10)-plane while chains from the (002)-plane are colinear with the (220)-plane. Angles formed between the chains and the *a* and *b* axes are 55.3° and 34.7° respectively. The acute angle between the criss-crossed chains is twice the angle formed with the *b*-axis or 2arctan(a/b) = 69.4°. The criss-cross arrangement gives rise to channels along the *c*-direction. The channels contain the hydroxide anion and the water of crystallization. The chains cross with their bipyridine ligands to yield a possible π−π stacking situation. The symmetry related pyridyl planes overlap with a sizable displacement angle of 40.8° at a centroid-centroid distance of 4.313 Å and an interplanar angle and separation of 19.0° and 3.26 Å, respectively (see also Fig. 4a). These π−π stacking parameters suggest only a weak stacking interaction [46]. A channel-containing 1D coordination polymer has also been prepared from $Cu_2(O_2CMe)_4$ and 1,3-di-4-pyridylpropane [47].

Chains from adjacent layers are hydrogen bonded across the acute angles between the chains (Fig. 4a). One of the hydrogen atoms of the aqua ligands interacts with an oxygen atom on the nitrato ligand. Furthermore, the same kind of hydrogen bonding also occurs to the next but one chain which is directly stacked on top by a translation of one unit-cell length along *c* (Fig. 4b).

The channels in **1** (Fig. 3) are not empty but filled with water molecules of crystallization and a hydroxide ion. Both species are highly disordered even at low temperature (−50 °C). The residual electron density in the channels could be refined to two oxygen atoms per iron atom which were distributed over five positions. Since this electron density was disordered along the channels even at low temperature the exact chemical composition could not be decided from crystallographic aspects alone. The decision coincided with the question if iron would be Fe^{II} or Fe^{III} (or mixed valent) in **1**.

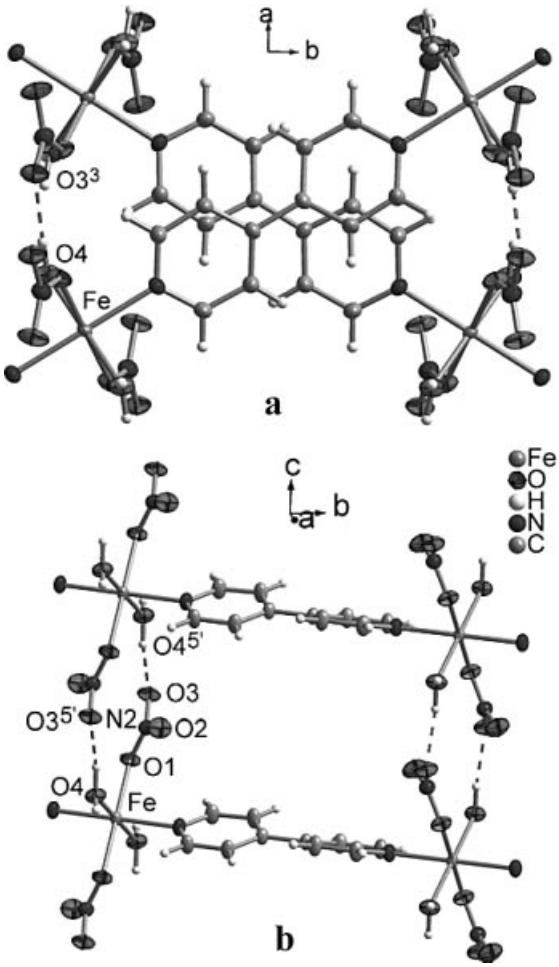

Fig. 4 (a) Hydrogen contact between directly adjacent criss-crossed chains in **1**; view along the *c* axis. (b) Hydrogen contact between next-nearest neighboring chains in **1** (related by translation along c). Distances (Å) and angles (°) for the hydrogen bonds:

D−H···A	D−H	H···A	D···A	D−H···A
O4−H4B···O3$^{5'}$	0.92(3)	1.94(3)	2.791(2)	154(3)
O4−H4C···O3^{3}	0.87(3)	1.90(3)	2.769(3)	175(3)

D = Donor, A = acceptor. Symmetry transformations: 3 = 0.5+x, 1−y, 0.5−z; 5′ = 1−x, 1−y, 1−z.

Thermogravimetric analysis shows a weight loss of about 9.0 % at 120 °C which corresponds to the loss of a hydroxide and a water molecule of crystallization (calculated 8.6 %). The hydroxide may be protonated to leave the lattice as a water molecule (calculated 8.8 %). A second weight loss between 260 and 290 °C of 58.5 % is assigned to the loss of the two aqua ligands, the bipyridine and one NO_2 from the decompositon of one nitrate (calculated 58.5 %). The remaining mass of about 32 % is assigned to $FeO(NO_3)$ (calculated 32.9 %).

Compound $^{1}_{\infty}\{[Fe^{II}(H_2PO_4)_2(\mu\text{-}4,4'\text{-bipy})(H_2O)_2]\cdot H_2O\cdot(4,4'\text{-bipy})\}$ (2)

Hydrothermal treatment of 4,4′-bipyridine with iron(II) acid chloride in the presence of phosphoric acid and tetra-n-butylammonium hydroxide in water at 165 °C yielded dark-red to red-brown, thick needle-shaped crystals which analyzed as the title compound **2** (eq. (2)) from Mössbauer and single-crystal X-ray diffraction.

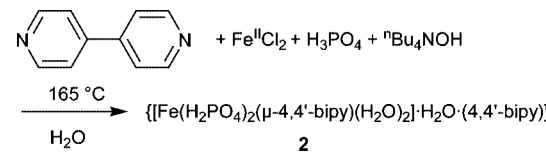

(2)

Again in the crystal structure the hydrogen atoms on the unligated oxygen atom could not be determined without ambiguity. Thus, as in **1**, an assignment as either a water molecule of crystallization (and Fe in oxidation state +II) or a hydroxide (and Fe in oxidation state +III) would have been possible. As before in **1**, ^{57}Fe Mössbauer spectroscopy was used to determine the iron oxidation state [38]. The Mössbauer spectra for compound **2** as a function of temperature, show only a single wide quadrupole doublet,

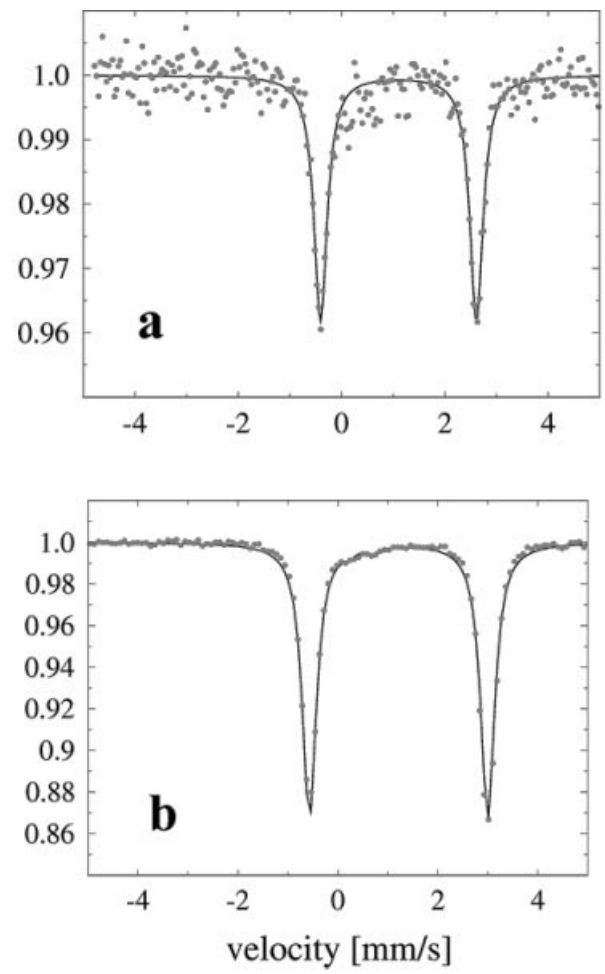

Fig. 5 Mössbauer spectra of $^{1}_{\infty}\{[Fe^{II}(H_2PO_4)_2(\mu\text{-}4,4'\text{-bipy})(H_2O)_2]\cdot H_2O\cdot(4,4'\text{-bipy})\}$ (**2**) at (a) room temperature and (b) T = 77 K. A sum of Lorentzians (solid lines) is used to fit the experimental data (dots); see text for individual parameters.

whose parameters exhibit some increase with temperature due to the second-order Doppler-effect and are clearly indicative of Fe^{II} in the high-spin state (Fig. 5) ($\delta^{\alpha-Fe}$ = 1.10 mm s^{-1}, ΔE_Q = 3.02 mm s^{-1} at RT; $\delta^{\alpha-Fe}$ = 1.21 mm s^{-1}, ΔE_Q = 3.56 mm s^{-1} at 77 K). A good agreement exists with the DFT-calculated Mössbauer parameters in Table 2 for a model compound with an FeO_4N_2 coordination sphere. A very small (around 2 %) low-spin contribution with $\delta^{\alpha-Fe}$ = 0.47 mm s^{-1}, ΔE_Q = 0.50 mm s^{-1} may be included in the spectrum at 77 K. For high-spin Fe^{II} in an FeO_4N_2 coordination environment an isomer shift around 1 mm s^{-1} and a quadrupole splitting above 2 mm s^{-1} is to be expected [30, 38].

The crystal structure of **2** consists of Fe-bipy chains. Each iron atom is *trans*-coordinated by two nitrogen donors from bridging bipyridine groups and *cis*-coordinated by two dihydrogenphosphate and two aqua ligands (Fig. 6). In addition there is an intra-chain hydrogen bond formation from the aqua ligand O10 to the oxygen atom O4 of the *cis*-positioned phosphate group. Bond distances and angles between non-hydrogen atoms are listed in Table 4. The 4,4′-bipyridine solvate molecule is also part of the one-dimensional chain construction (Fig. 7). It is held by hydrogen bonding between the H_2PO_4 groups on adjacent iron centers along the chain and is situated in a π−π contact to the coordinated 4,4′-bipy ligand. The 4,4′-bipyridine solvate molecule crosses the metal bridging 4,4′-bipyridine with an angle of 40° between the two N···N axes. The pyridyl planes from N1 and N3 overlap with a small displacement angle of 21.8° at a centroid-centroid distance of 3.586 Å and an interplanar angle and separation of 6.8° and 3.33 to 3.44 Å, respectively. The pyridyl planes from N2 and N4 also overlap with a small displacement angle of 20.1° at a centroid-centroid distance of 3.612 Å and an interplanar angle and separation of 3.7° and 3.39 Å, respectively. These parameters are at the strong end of a typical π−π stacking interaction [46]. There is a second π−π contact between the pyridyl plane from N4 to the one of N2 from a neighboring chain along *a* (Fig. 8). This inter-chain π-contact is somewhat longer than the intra-chain one, yet, still clearly within the normal range of a typical π-contact between aromatic nitrogen containing ligands [46], with a displacement angle of 23.4°, a centroid-centroid distance of 3.744 Å, an interplanar angle and separation of 3.7° and 3.44 to 3.52 Å, respectively.

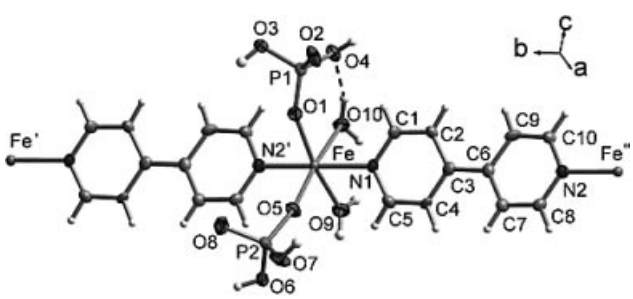

Fig. 6 Section of a single chain of $[Fe^{II}(H_2PO_4)_2(\mu\text{-}4,4'\text{-bipy})(H_2O)_2]$ in **2** constructed through the bridging action of one of the 4,4′-bipyridine ligands. The Fe-bipy chains extend along the *b*-direction. Symmetry transformations: ′ = x, 1+y, z; ″ = x, −1+y, z.

Table 4 Selected bonds lengths/Å and angles/° in compound **2** [a)]

Fe-O5	2.034(5)	Fe-O10	2.169(5)
Fe-O1	2.063(5)	Fe-N1	2.180(5)
Fe-O9	2.104(5)	Fe-N2′	2.183(5)
P1-O1	1.482(5)	P2-O5	1.491(5)
P1-O2	1.519(5)	P2-O6	1.505(5)
P1-O3	1.554(5)	P2-O7	1.558(5)
P1-O4	1.577(5)	P2-O8	1.574(5)
O5-Fe-O1	101.3(2)	O9-Fe-N1	86.0(2)
O5-Fe-O9	90.9(2)	O10-Fe-N1	89.0(2)
O1-Fe-O9	167.7(2)	O5-Fe-N2′	93.6(2)
O5-Fe-O10	172.8(2)	O1-Fe-N2′	90.2(2)
O1-Fe-O10	85.8(2)	O9-Fe-N2′	90.5(2)
O9-Fe-O10	82.0(2)	O10-Fe-N2′	87.5(2)
O5-Fe-N1	89.6(2)	N1-Fe-N2′	175.3(2)
O1-Fe-N1	92.6(2)		

[a)] Symmetry transformation: ′ = x, 1+y, z.

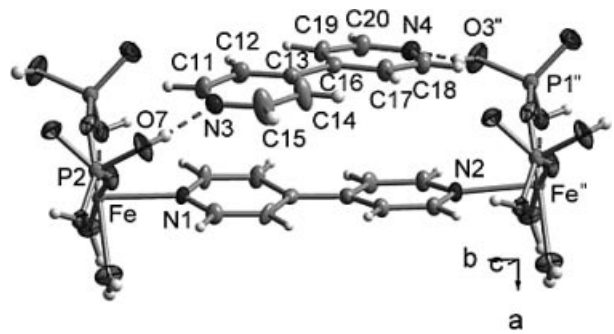

Fig. 7 Section of a single chain of $[Fe^{II}(H_2PO_4)_2(\mu\text{-}4,4'\text{-bipy})(H_2O)_2]\cdot(4,4'\text{-bipy})$ in **2** showing both the metal-coordinated and the hydrogen-bonded 4,4′-bipyridine solvate; see Table 5 for hydrogen bonding parameters. Symmetry transformation: ″ = x, −1+y, z.

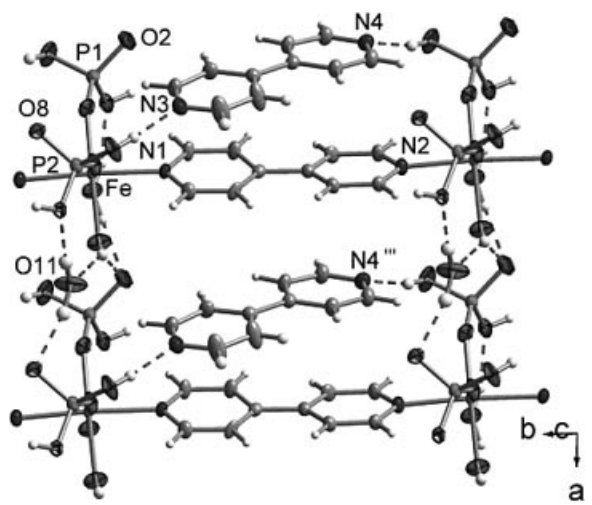

Fig. 8 Two neighboring Fe-bipy-chains in **2** with the second π-contact between the pyridyl rings of N2 and N4‴ along *a*. Symmetry transformation: ‴ = 1+x, y, z.

Adjacent Fe-bipy-chains are joined to a three-dimensional supramolecular network through hydrogen bonding. The chains are connected through complementary H-bonds between symmetry related dihydrogenphosphato groups; that is from O4 to O2 around P1 and from O6 to O8 around P2 (Fig. 9). The hydrogen bonding also involves the aqua ligand O9 which is binding to the water of crystallization (O11) and to O2 on P1. Also, the remaining hydrogen atom of the aqua ligand O10 binds to an adjacent O2 which, thereby, accepts two hydrogen bonds. Fig. 8 and 9 also depict the water of crystallization (O11) which was omitted in Fig. 6 and 7 for clarity. The water molecule of crystallization also interconnects the Fe-bipy-chains along the *a*-direction through hydrogen bonding to O8 and O6 on neighboring chains. The phosphate-water hydrogen-bonding network alone forms corrugated planes approximately parallel to the (011)-plane (Fig. 9 right). Details of the hydrogen-bonding scheme are provided in Table 5. For comparison, infinite M-bipy-M chains, similarly interconnected through hydrogen bonding are formed in $^{1}_{\infty}$\{[Co(SO$_4$)(μ-4,4′-bipy)-(H$_2$O)$_3$]·2H$_2$O\} [48].

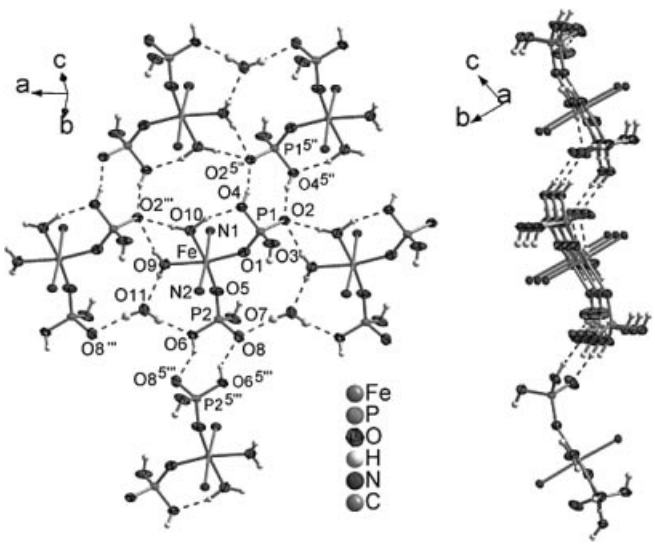

Fig. 9 Section of the hydrogen-bonded nets in **2**; left: on-top view, right: side-view; see Table 5 for hydrogen bonding parameters. Symmetry transformations: $''' = 1+x, y, z$; $5'' = -x, 1-y, 1-z$; $5''' = 1-x, 2-y, -z$;

We note that the color of iron(II) and iron(III) complexes in a ligand field of two nitrogen and four oxygen donors (FeO_4N_2 coordination sphere) can vary to a large extent from (dark-)red [49] over brown [50] to (red-)orange(-yellow) [51] and even light-/yellow-green [52] for Fe^{II} and from (dark-)blue [53], (dark-)red [54] to orange/yellow [55] and (dark-)green [56] for Fe^{III}.

Polarized elctronic absorption spectra of arbitrary crystal faces of **1** and **2** (Fig. 10) have been measured at 293 K using a special microcrystal-UV/VIS-spectrophotometer. The absorption spectra of **1** (chromophor [$Fe^{III}N_2O_4$]) show one broad band around 21000 cm^{-1}, probably consisting of two components (20500 and 22000 cm^{-1}). Above

Table 5 H-bonding distances/Å and angles/° in compound **2** [a)]

D-H···A	D-H	H···A	D···A	D-H···A
intra-chain H-bond (cf. Fig. 6):				
O10-H10B···O4	0.99	1.88	2.838(7)	161.4
hydrogen bonding to 4,4′-bipy (cf. Fig. 7):				
O3-H3A···N4′	0.83	1.77	2.578(7)	165.5
O7-H7A···N3	0.83	1.80	2.619(7)	170.3
inter-chain H-bonds (cf. Fig. 9):				
O4-H4A···O2$^{5''}$	0.83	1.73	2.540(6)	163.1
O6-H6A···O8$^{5'''}$	0.83	1.82	2.532(7)	142.5
O9-H9B···O2$'''$	0.84	2.00	2.821(7)	167.0
O10-H10A···O2$'''$	0.92	1.87	2.793(7)	177.1
··· involving the water of crystallization (O11) (cf. Fig. 9)				
O9-H9A···O11	0.84	1.91	2.628(7)	143.0
O11-H11B···O6	0.87	1.83	2.696(8)	169.8
O11-H11A···O8$'''$	0.92	1.91	2.815(8)	166.3

[a)] D = Donor, A = acceptor. For found and refined atoms the standard deviations are given. Symmetry transformations: $' = x, 1+y, z$; $''' = 1+x, y, z$; $5'' = -x, 1-y, 1-z$; $5''' = 1-x, 2-y, -z$.

24000 cm^{-1} the onset of the charge transfer region is observed. Unambigous assignment of the band around 21000 cm^{-1} is impossible. Three different types of transition appear to be reasonable as explanation: $^6A_{1g}\rightarrow{}^4T_{1g}(^4G)$ for high-spin Fe^{3+}, $^2T_{2g}\rightarrow{}^2A_{2g}$, $^2T_{1g}$ for low-spin Fe^{3+}, or a LMCT from 4,4′-bipyridine ligand to the iron(III) cation.

The absorption spectra of **2** (chromophor [$Fe^{II}N_2O_4$]) show a broad absorption band at 12000 cm^{-1} which is assigned to the spin-allowed $^5T_{2g}\rightarrow{}^5E_g$ transition of high-spin iron(II) in octahedral environment. In one polarisation direction ("hpol") a clearly visible shoulder in the absorption curve is observed at 16000 cm^{-1}. This shoulder is completely extinguished in the second polarisation direction ("vpol", Fig. 10), explaining the observed dichroism. The energy and strong polarisation behavior of the absorption at 16000 cm^{-1} points to its origin from a charge transfer transition $Fe^{2+}\leftrightarrow$4,4′-bipyridine, in agreement with the almost perfect alignment of all bonds Fe−N parallel to the crystallographic *b*-axis. The noise observed at higher wavenumbers for both polarisation directions is due to the almost complete absorption of light.

Experimental part

IR spectra (KBr pellet) were measured on a Bruker Optik IFS 25. Elemental analyses were obtained on a VarioEL from Elementaranalysensysteme GmbH. Iron analyses were carried out by atomic absorption spectroscopy on a Vario 6 flame photometer from Analytik Jena. $Fe(NO_3)_3\cdot 9H_2O$ and $FeCl_2\cdot 3H_2O$ were obtained from Merck, the solution of $^nBu_4NOH$ (40 wt% in water, d = 0.990 g/mL, 0.65 mmol/mL) from Aldrich. Thermogravimetric analysis was done on a simultaneous thermoanalysis apparatus STA 409 from Netzsch under nitrogen.

^{57}Fe Mössbauer spectroscopy

^{57}Fe Mössbauer spectra were recorded with a conventional spectrometer in constant-acceleration mode with a ^{57}Co[Rh] source.

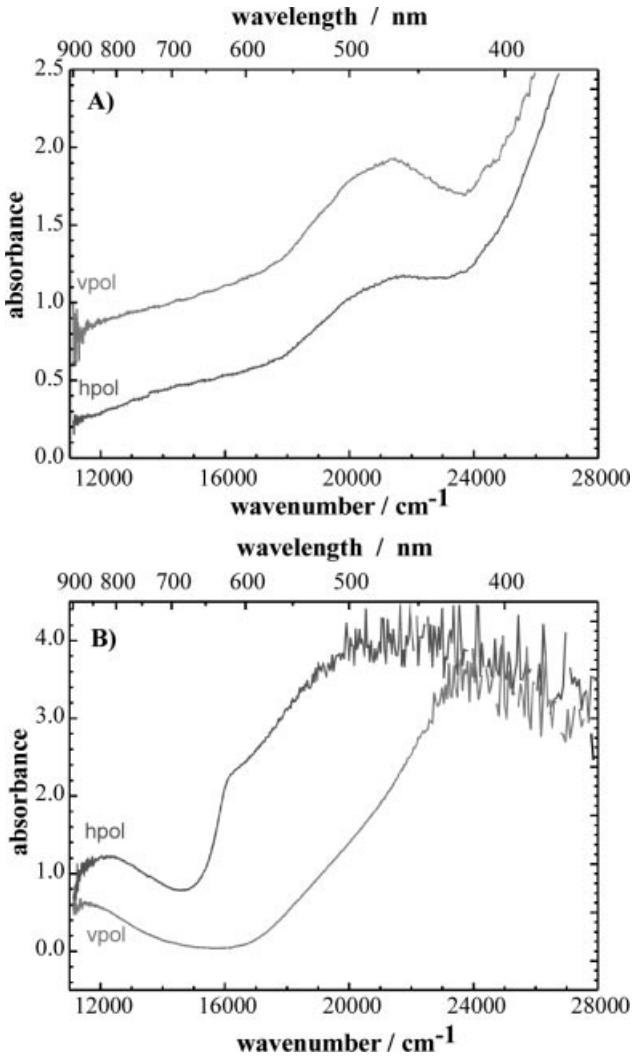

Fig. 10 Polarized single crystal electronic absorption spectra of **1** (A) and **2** (B) in the visible region.

The velocity calibration was performed with an α-Fe foil at room temperature, for which the magnetic hyperfine splitting is known with high accuracy. The measured isomer shifts are referred to this α-Fe standard. The experimental spectra were fitted by a sum of Lorentzian lines by means of a least-squares procedure.

DFT calculations

The geometry of trans-$[Fe(NO_3)_2(H_2O)_2(pyridine)_2]$ as a simple model for **1** has been optimized using the hybrid method B3LYP (Becke's three parameter hybrid functional [57] using Lee, Yang, and Parr's correlation functional [58, 59]) together with the all-electron 6-311G basis for H, C, and N and the Wachters-Hay double-ζ basis for Fe [60, 61] as included in the program packages Gaussian 98, Rev. A11.4 [62]. The calculations have been performed for a neutral and a positively charged model with different total spin (S = 0 and S = 2 in the first case, S = 1/2 and S = 5/2 in the second case). The resulting charge distributions at the iron center correspond to Fe(II) and Fe(III) in the low-spin and high-spin states. The quadrupole splitting ΔE_Q has been derived from the largest component V_{zz} and the asymmetry parameter η of the calculated traceless electric field gradient tensor using the relation [63] $\Delta E_Q = {}^1/_2 eQ\ V_{zz}\ \sqrt{1+\Sigma\eta^2}$ and the nuclear quadrupole moment Q = 0.16 barn [64]. The isomer shift δ had been derived from the nonrelativistic electronic charge density at the iron nucleus according to the relation [63] $\delta = -1.3\ \alpha(\rho - c)$ using α = 0.28 mm s^{-1} e^{-1} $a_0{}^3$ and setting c = 11617 e $a_0{}^{-3}$.

Optical spectroscopy

Details on the microcrystal-UV/VIS-spectrophotometer have already been published elsewhere [65]. Crystals of **1** are orange, those of **2** show dichroic (dark red / orange) behaviour. Crystals under investigation had a thickness of 0.2 mm. The cross-section of the light beam was 0.03 mm^2.

X-ray Crystallography

Data Collection: Bruker AXS with CCD area-detector, Mo-Kα radiation (λ = 0.71073 Å), graphite monochromator, double-pass method ϕ−ω-scan, Data collection and cell refinement with SMART [66], data reduction with SAINT [66], experimental absorption correction with SADABS [67] *Structure Analysis and Refinement*: The structure was solved by direct methods (SHELXS-97) [68]; refinement was done by full-matrix least squares on F^2 using the SHELXL-97 program suite [68]. All non-hydrogen positions were found and refined with anisotropic temperature factors. In **1** the hydrogen atoms of the aqua ligands were found and refined with Ueq(H) = 1.2 Ueq(O). The hydroxide and water molecule of crystallization (O51−O55) are disordered, their hydrogen atoms were neither found nor calculated. In **2** the hydrogen atoms of the water of crystallization (O11), the two aqua ligands (O9 and O10) were initially found from the difference Fourier map but had to be fixed (AFIX 1) in the subsequent refinement; Ueq(H) = 1.5Ueq(O). The hydrogen atoms on the phosphate ligands were placed in calculated positions with the appropriate riding model AFIX 147 and Ueq(H) = 1.5Ueq(O). In **1** and **2** hydrogen atoms on the bipyridine ligand were placed in calculated position with the appropriate riding model AFIX 43 and Ueq(H) = 1.2Ueq(C). Graphics were obtained with DIAMOND [69]. Crystal data and details on the structure refinement are given in Table 6. The structural data has been deposited with the Cambridge Crystallographic Data Center (CCDC-No. 210646 and 210647).

Synthesis

Catena-{diaqua-(μ-4,4′-biypridine)-dinitrato-iron(III)-hydroxide hydrate}, $^1_\infty\{[Fe^{III}(NO_3)_2(\mu\text{-}4,4'\text{-bipy})(H_2O)_2]OH{\cdot}H_2O\}$, (1). In a Schlenk flask under a positive pressure of argon $Fe(NO_3)_3{\cdot}9H_2O$ (0.404 g, 1.00 mmol) and 4,4′-bipyridine (0.156 g, 1.00 mmol) were dispersed in 7 mL of degassed water resulting a yellowish slurry. To this slurry was added 1.3 mL of a 40 wt% solution of tetra-n-butyl ammonium hydroxide in water (2.0 mmol). The mixture was transferred to a Teflon-lined stainless-steel autoclave and heated at 165 °C for 48 h followed by slow cooling at a rate of 10 °C/h. Light-orange crystals were collected by filtration (yield 125 mg, 31 %). Calc. for $C_{10}H_{15}FeN_4O_{10}$ (407.09): C 29.50, H 3.71, N 13.76, Fe 13.72. Found C 28.76, H 3.57, N 13.04, Fe 13.95 %.

IR (KBr, major peaks only, cm^{-1}): 3330 (br, νOH), 1599 (νC=C), 1406 (νN=O), 999 (νN-O).

Table 6 Crystal data for compounds **1** and **2**

	1	**2**
Formula	$C_{10}H_{12}FeN_4O_{10}$ [a]	$C_{20}H_{26}FeN_4O_{11}P_2$
M	404.09	616.24
Crystal size/mm	0.16x0.14x0.14	0.2x0.2x0.2
Crystal description	isometric	isometric
T/K	223(2)	213(2)
θ range/°	2.09−28.86	1.39−25.80
h; k; l range	−15, 15; −24, 26; −10, 10	−8, 8; −14, 13; −18, 18
Crystal system	orthorhombic	triclinic
Space group	Pccn	$P\bar{1}$
a /Å	11.808(2)	7.1731(19)
b /Å	19.487(4)	11.4726(3)
c /Å	7.4073(15)	15.109(4)
α /°		78.661(4)
β /°		82.368(4)
γ /°		87.230(4)
V /Å^3	1704.4(6)	1207.9(6)
Z	4	2
D /g cm^{-3}	1.575	1.694
F(000)	824	636
μ /mm^{-1}	0.942	0.827
Absorption correction	SADABS	SADABS
Max/min transmission	0.8794/0.8638	0.9837/0.8521
Measured reflections	14102	9445
Unique reflections (R_{int})	2110 (0.0320)	4604 (0.0399)
Obs. reflects [$I > 2\sigma(I)$]	1497	3177
Parameters refined	130	348
Max/min $\Delta\rho$ /e Å^{-3} [b]	0.842/−0.450	1.945/−0.718
$R1$/$wR2$ [$I > 2\sigma(I)$] [c]	0.0430/0.1136	0.0693/0.2135
$R1$/$wR2$ (all data) [c]	0.0601/0.1249	0.0956/0.2280
Goodness-of-fit on F^2 [d]	1.020	1.093
Weight. scheme w; a/b [e]	0.0701/0.7144	0.1006/5.3318

[a] The hydroxide and water molecule of crystallization are disordered, their hydrogen atoms were neither found nor calculated, hence there is a deviation of three hydrogen atoms in the chemical formula from X-ray diffraction and the analytical chemical formula − [b] Largest difference peak and hole − [c] $R1 = [\Sigma(\|F_o| - |F_c\|)/\Sigma|F_o|]$; $wR2 = [\Sigma[w(F_o^2 - F_c^2)^2]/\Sigma[w(F_o^2)^2]]^{1/2}$ − [d] Goodness-of-fit = $[\Sigma[w(F_o^2 - F_c^2)^2]/(n-p)]^{1/2}$ − [e] $w = 1/[\sigma^2(F_o^2) + (aP)^2 + bP]$ where $P = (\max(F_o^2 \text{ or } 0) + 2F_c^2)/3$.

Catena-{diaqua-(μ-4,4′-biypridine)-bis(dihydrogenphosphato)-iron(II)-hydrate 4,4′-bipyridine solvate}, $^1_\infty${[$Fe^{II}(H_2PO_4)_2$(μ-4,4′-bipy)$(H_2O)_2$]·H_2O·(4,4′-bipy)}, (2). In a Schlenk flask under a positive pressure of argon $FeCl_2 \cdot 3H_2O$ (0.235 g, 1.00 mmol) and 4,4′-bipyridine (0.156 g, 1.00 mmol) were dispersed in 7 mL of degassed water resulting in a yellowish green slurry. To this slurry was carefully added 2.35 mL of a 1 mol/L solution of H_3PO_4 to completely dissolve the 4,4′-bipy. The pH value was set to 4.3 using 0.5 mL of a 40 wt% solution of tetra-n-butyl ammonium hydroxide in water. The solution was stirred for 30 min, transferred to a Teflon-lined stainless-steel autoclave and heated at 165 °C for 48 h followed by slow cooling at a rate of 10 °C/h. Dark-red crystals were collected by filtration (yield 275 mg, 44 %). Calc. for $C_{20}H_{26}FeN_4O_{11}P_2$ (616.24): C 38.98, H 4.25, N 9.09, Fe 9.06. Found C 38.76, H 4.48, N 9.04, Fe 9.18 %.

IR (KBr, major peaks only, cm^{-1}): 3505 (br, νOH), 1604 (νC=C), 1412 (νP=O), 948 (νP-O).

Acknowledgement. The research was supported by the Fonds der Chemischen Industrie and the graduate college "Unpaired electrons" at the University of Freiburg through a fellowship to *K. A.-S.* We thank *Prof. A. X. Trautwein*, Universität zu Lübeck for his support and helpful discussions.

References

[1] C. Janiak, *Dalton Trans.* **2003**, 2781.
[2] See Table 2 in P. J. Hagrman, D. Hagrman, J. Zubieta, *Angew. Chem. Int. Ed. Engl.* **1999**, *38*, 2638.
[3] B. Moulton, M. J. Zaworotko, *Chem. Rev.* **2001**, *101*, 1629.
[4] For long bis(4-pyridyl) ligands, see S. Banfi, L. Carlucci, E. Caruso, G. Ciani, D. M. Proserpio, *J. Chem. Soc., Dalton Trans.* **200 2**, 2714. K. Biradha, M. Fujita, *Chem. Commun.* **2001**, 15. H.-P. Wu, C. Janiak, L. Uehlin, P. Klüfers, P. Mayer, *Chem. Commun.* **1998**, 2637. D. M. Curtin, Y.-B. Dong, M. D. Smith, T. Barclay, H.-C. zur Loye, *Inorg. Chem.* **2001**, *40*, 2825. S. R. Seidel, F. M. Tabellion, A. M. Arif, P. J. Stang, *Isr. J. Chem.* **2001**, *41*, 149; S. R. Batten, B. F. Hoskins, B. Moubaraki, K. S. Murray, R. Robson, *Chem. Commun.* **2000**, 1095. K. Kasai, M. Aoyagi, M. Fujita, *J. Am. Chem. Soc.* **2000**, *122*, 2140. B.-L. Fei, W.-Y. Sun, K.-B. Yu, W.-X. Tang, *J. Chem. Soc., Dalton Trans.* **2000**, 805.
[5] For multimodal derivatives of pyridyl ligands, see N. S. Oxtoby, A. J. Blake, N. R. Champness, C. Wilson, *Proc. Natl. Acad. Sci. USA* **2002**, *99*, 4905. C. Janiak, L. Uehlin, H.-P. Wu, P. Klüfers, H. Piotrowski, T. G. Scharmann, *J. Chem. Soc., Dalton Trans.* **1999**, 3121. A. J. Blake, N. R. Champness, P. Hubberstey, W.-S. Li, M. A. Withersby, M. Schröder, *Coord. Chem. Rev.* **1999**, *183*, 117.
[6] $^1_\infty${$Zn(NCS)_2$(μ-4,4′-bipy)}, $^1_\infty${[$(Zn(SO_4)$(μ-4,4′-bipy)$(H_2O)_3)$]·$3H_2O$}: M. Kondo, M. Shimamura, S.-I. Noro, T. Yoshitomi, S. Minakoshi, S. Kitagawa, *Chem. Lett*. **1999**, 285
[7] $Ni_2(NO_3)_4$(μ-4,4′-bipy)$_3$: E. J. Cussen, J. B. Claridge, M. J. Rosseinsky, C. J. Kepert, *J. Am. Chem. Soc.* **2002**, *124*, 9575
[8] Feature article: M. J. Zaworotko, *Chem. Commun.* **2001**, 1.
[9] $^2_\infty${$[Cd(NO_3)_2$(μ-4,4′-bipy$)_2(H_2O)_2]\cdot 1.5(C_6H_4Br_2)_2$}: M. Fujita, Y. Kwon, S. Washizu, K. Ogura, *J. Am. Chem. Soc.* **1994**, *116*, 1151.
[10] $^2_\infty${$[Cu^I_2Cu^{II}$(diphosphonate)(μ-4,4′-bipy)2]·$2H_2O$}: L.-M. Zheng, P. Yin, X.-Q. Xin, *Inorg. Chem.* **2002**, *41*, 4084.
[11] $^2_\infty${$[Cu_2$(malonato$)_2$(μ-4,4′-bipy$)(H_2O)_2]\cdot H_2O$}: J.-M. Li, Y.-G. Zhang, J.-H. Chen, L. Rui, Q.-M. Wang, X.-T. Wu, *Polyhedron* **2000**, *19*, 1117. J. Li, H. Zeng, J. Chen, Q. Wang, X. Wu, *Chem. Commun.* **1997**, 1213.
[12] $^2_\infty[Cu_2X_2$(4,4′-bipy)] (X = Cl, Br) and $^2_\infty$[CuBr(4,4′-bipy)]: J. Y. Lu, B. R. Cabrera, R.-J. Wang, J. Li, *Inorg. Chem.* **1999**, *38*, 4608.
[13] $^2_\infty${$[Cu$(μ-4,4′-bipy)(pyrazine)$(H_2O)_2][PF_6]_2$}: M.-L. Tong, X.-M. Chen, X.-L. Yu, T. C. W. Mak, *J. Chem. Soc., Dalton Trans.* **1998**, 5.
[14] $^3_\infty${$[Cu_3$(μ-4,4′-bipy$)_5$(MeCN$)_2]PW_{12}O_{40}\cdot 2$PhCN}: C. Inman, J. M. Knaust, S. W. Keller, *Chem. Commun.* **2002**, 156.
[15] $^3_\infty${$[Zn(SiF_6)_2$(μ-4,4′-bipy$)_2]\cdot x$DMF}: S. Subramanian, M. Zawarotko, *Angew. Chem., Int. Ed. Engl*. **1995**, *34*, 2127.
[16] $^3_\infty$[Co(phthalato$)_2$(μ-4,4′-bipy)] and $^3_\infty[Co_2$(malonato$)_2$(μ-4,4′-bipy$)(H_2O)_2$]: P. Lightfoot, A. Snedden, *J. Chem. Soc., Dalton Trans.* **1999**, 3549.
[17] K. Abu-Shandi, C. Janiak, B. Kersting, *Acta Crystallogr. C* **2001**, *57*, 1261.
[18] $^1_\infty${$[Ni(ClO_4)_2$(μ-4,4′-bipy$)_{2.5}(H_2O)_2]\cdot 1.5$(4,4′-bipy)$\cdot 2H_2O$}: O. M. Yaghi, H. Li, T. L. Groy, *Inorg. Chem.* **1997**, *36*, 4292.
[19] $^1_\infty${$[Co(H_2O)_4$(μ-4,4′-bipy)$][PF_6]_2\cdot 3$(4,4′-bipy)}: Y.-B. Dong, M. D. Smith, R. C. Layland, H.-C. zur Loye, *J. Chem. Soc., Dalton Trans.* **2000**, 775.
[20] Molecular [Mn(μ-4,4′-bipy$)_2(H_2O)_4][ClO_4]_2\cdot$4(4,4′-bipy): M.-L. Tong, H. K. Lee, X.-M. Chen, R.-B. Huang, T. C. W. Mak, *J. Chem. Soc., Dalton Trans.* **1999**, 3657.

[21] $^{1}_{\infty}$\{[Zn(μ-4,4′-bipy)$(H_2O)_4$]X_2·4,4′-bipy or 2(4,4′-bipy)·$3H_2O$\} (X = NO_3, O_3SCF_3) and $^{1}_{\infty}$\{[Fe(ClO_4)(μ-4,4′-bipy)$(H_2O)_3$]-ClO_4·H_2O·1.5(4,4′-bipy)\}: L. Carlucci, G. Ciani, D. M. Proserpio, A. Sironi, *J. Chem. Soc., Dalton Trans.* **1997**, 1801.

[22] S.-I. Noro, M. Kondo, T. Ishii, S. Kitagawa, H. Matsuzaka, *J. Chem. Soc., Dalton Trans.* **1999**, 1569.

[23] N. Moliner, M. Carmen Munoz, J. A. Real, *Inorg. Chem. Commun.* **1999**, *2*, 25.

[24] N. Moliner, M. C. Munoz, S. Letard, L. Salmon, J.-P. Tuchagues, A. Bosseksou, J. A. Real, *Inorg. Chem.* **2002**, *41*, 6997.

[25] G. S. Matouzenko, G. Molnar, N. Brefuel, M. Perrin, A. Bousseksou, S. A. Borshch, *Chem. Mater.* **2003**, *15*, 550.

[26] A. Panda, M. Stender, M. M. Olmstead, P. Klavins, P. P. Power, *Polyhedron* **2003**, *22*, 67.

[27] P. Jensen, S. R. Batten, B. Moubaraki, K. S. Murray, *J. Chem. Soc., Dalton Trans.* **2002**, 3712.

[28] M. A. Lawandy, X. Huang, R.-J. Wang, J. Li, J. Y. Lu, T. Yuen, C. L. Lin, *Inorg. Chem.* **1999**, *38*, 5410.

[29] J. Y. Lu, M. A. Lawandy, J. Li, T. Yuen, C. L. Lin, *Inorg. Chem.* **1999**, *38*, 2695.

[30] L.-M. Zheng, X. Fang, K.-H. Lii, H.-H. Song, X.-Q. Xin, H.-K. Fun, K. Chinnakali, I. A. Razak, *J. Chem. Soc., Dalton Trans.* **1999**, 2311.

[31] J. Greve, I. Jess, C. Näther, *J. Solid State Chem.* **2003**, *175*, 328. S. Konar, M. Corbella, E. Zangrando, J. Ribas, N. R. Chaudhuri, *Chem. Commun.* **2003**, 1424.

[32] Y.-Y. Chen, B. Zhao, P. Cheng, B. Ding, D.-Z. Liao, S.-P. Yan, Z.-H. Jiang, *Eur. J. Inorg. Chem.* **2004**, 562.

[33] S.-I. Noro, M. Kondo, S. Kitagawa, T. Ishii, H. Matsuzaka, *Chem. Lett.* **1999**, 727.

[34] A. Fu, X. Huang, J. Li, T. Yuen, C. L. Lin, *Chem. Eur. J.* **2002**, *8*, 2239.

[35] S. Martin, M. G. Barandika, J. M. Ezpeleta, R. Cortes, J. I. Ruiz de Larramendi, L. Lezama, T. Rojo, *J. Chem. Soc., Dalton Trans.* **2002**, 4275.

[36] N. Moliner, J. A. Real, M. C. Muñoz, R. Martínez-Mañez, J. M. C. Juan, *J. Chem. Soc., Dalton Trans.* **1999**, 1375. R. E. Marsh, *Acta Crystallogr.* **2004**, *B60*, 252.

[37] P. A. M. Williams, E. G. Ferrer, E. J. Baran, O. E. Piro, J. A. Ellena, E. E. Castellano, *An. Asoc. Quim. Argent.* **2002**, *90*, 109.

[38] N. N. Greenwood, T. C. Gibb, *Mössbauer Spectroscopy*, Chapman and Hall, London 1971.

[39] Recent monographs: *Topics Curr. Chem.* **2004**, *233−235 (Spin Crossover in Transition Metal Compounds I − III*; P. Gütlich, H. A. Goodwin, eds.), Springer, Berlin, 2004.

[40] Reviews: P. Gütlich, A. Hauser, H. Spiering, *Angew. Chem.* **1994**, *106*, 2109; *Angew. Chem. Int. Ed. Engl.* **1994**, *33*, 2024. O. Kahn, Molecular Magnetism, VCH, Weinheim, 1993, ch. 4, p. 53ff. J. Zarembowitch, *New. J. Chem.* **1992**, *16*, 255. P. Gütlich, A. Hauser, *Coord. Chem. Rev.* **1990**, *97*, I. H. Toftlund, *Coord. Chem. Rev.* **1989**, *94*, 67. E. König, *Progr. Inorg. Chem.* **1987**, *35*, 527. P. Gütlich, *Struct. Bonding* (Berlin) **1981**, *44*, 83. H. A. Goodwin, *Coord. Chem. Rev.* **1976**, *18*, 293.

[41] C. Janiak, T. G. Scharmann, T. Bräuniger, J. Holubova, M. Nadvornik, *Z. Anorg. Allg. Chem.* **1998**, *624*, 769; C. Janiak, T. G. Scharmann, J. C. Green, R. P. G. Parkin, M. J. Kolm, E. Riedel, W. Mickler, J. Elguero, R. M. Claramunt, D. Sanz, *Chem. Eur. J.* **1996**, *2*, 992.

[42] B. Kersting, M. J. Kolm, C. Janiak, *Z. Anorg. Allg. Chem.* **1998**, **624**, 775. B. Kersting, D. Siebert, D. Volkmer, M. J. Kolm, C. Janiak, *Inorg. Chem.* **1999**, *38*, 3871.

[43] A. Geiß, M. J. Kolm, C. Janiak, H. Vahrenkamp, *Inorg. Chem.* **2000**, *39*, 4037.

[44] $^{3}_{\infty}$[$Mn(N_3)_2$(4,4′-bipy)] and other extended azido structures: S. Han, J. L. Manson, J. Kim, J. S. Miller, *Inorg. Chem.* **2000**, *39*, 4182; and references therein.

[45] $^{3}_{\infty}$[$Co(dca)_2$(4,4′-bipy)]: B.-W. Sun, S. Gao, B.-Q. Ma, Z.-M. Wang, *New J. Chem.* **2000**, *24*, 953.

[46] C. Janiak, *J. Chem. Soc., Dalton Trans.* **2000**, 3885.

[47] W. J. Belcher, C. A. Longstaff, M. R. Neckenig, J. W. Steed, *Chem. Commun.* **2002**, 1602.

[48] $^{1}_{\infty}$\{$Co(CH_3COO)_2$(μ-4,4′-bipy)\}: J. Lu, C. Yu, T. Niu, T. Paliwala, G. Crisci, F. Somosa, A. J. Jacobson, *Inorg. Chem.* **1998**, *37*, 4637.

[49] L.-M. Zheng, X. Fang, K.-H. Lii, H.-H. Song, X.-Q. Xin, H.-K. Fun, K. Chinnakali, I. A. Razak, *J. Chem. Soc., Dalton Trans.* **1999**, 2311. N. Okabe, T. Makino, *Acta Crystallogr.* **1998**, *C54*, 1279; P. Laine, A. Gourdon, J.-P. Launay, *Inorg. Chem.* **1995**, *34*, 5129. P. Laine, A. Gourdon, J.-P. Launay, *Inorg. Chem.* **1995**, *34*, 5138.

[50] J. Sletten, H. Daraghmeh, F. Lloret, M. Julve, *Inorg. Chim. Acta* **1998**, *127*, 279. E. Andres, G. De Munno, M. Julve, J. A. Real, F. Lloret, *J. Chem. Soc., Dalton Trans.* **1993**, 2169.

[51] Q. Liu, Y. Wei, W. Wang, S. Zhang, *Acta Crystallogr.* **1999**, *C55*, 9900127. S. Noro, M. Kondo, S. Kitagawa, T. Ishii, H. Matsuzaka, *Chem. Lett.* **1999**, 727. J. M. C.-Juan, C. Mackiewicz, M. Verelst, F. Dahan, A. Bousseksou, Y. Sanakis, J.-P. Tuchagues, *Inorg. Chem.* **2002**, *41*, 1478.

[52] M. Tiliakos, P. Cordopatis, A. Terzis, C. P. Raptopoulou, S. P. Perlepes, E. M. Zoupa, *Polyhedron* **2001**, *20*, 2203. S. Kiani, A. Tapper, R. J. Staples, P. Stavropoulos, *J. Am. Chem. Soc.* **2000**, *122*, 7503.

[53] A. Neves, M. A. de Brito, I. Vencato, V. Drago, K. Griesar, W. Haase, Y. P. Mascarenhas, *Inorg. Chim. Acta* **1993**, **2**, 214. A. Neves, M. A. de Brito, I. Vencato, V. Drago, K. Griesar, W. Haase, *Inorg. Chem.* **1996**, *35*, 2360. D. Zirong, S. Bhattacharya, J. K. McCusker, P. M. Hagen, D. N. Hendrickson, C. G. Pierpont, *Inorg. Chem.* **1992**, *31*, 870.

[54] Y. Feng, S-L. Ong, J. Hu, W-J. Ng, *Acta Crystallogr.* **2002**, *C58*, m34. A. Horn, A. Neves, A. J. Bortoluzzi, V. Drago, W. A. Ortiz, *Inorg. Chem. Commun.* **2001**, *4*, 173. E. J. Seddon, J. Yoo, K. Folting, J. C. Huffman, D. N. Hendrickson, G. Christou, *J. Chem. Soc., Dalton Trans.* **2000**, 3640. C. M. Grant, M. J. Knapp, J. C. Huffman, D. N. Hendrickson, G. Christou, *Chem. Commun.* **1998**, 1753. C. M. Grant, M. J. Knapp, W. E. Streib, J. C. Huffman, D. N. Hendrickson, G. Christou, *Inorg. Chem.* **1998**, *37*, 6065. S. M. Gorun, S. J. Lippard, *Inorg. Chem.* **1988**, *27*, 149. A. J. Blake, C. M. Grant, S. Parsons, G. A. Solan, R. E. P. Winpenny, *J. Chem. Soc., Dalton Trans.* **1996**, 321.

[55] R. W. Saalfrank, I. Bernt, M. M. Chowdhry, F. Hampel, G. B. M. Vaughan, *Chem. Eur. J.* **2001**, *7*, 2765. E. J. Seddon, J. C. Huffman, G. Christou, *J. Chem. Soc., Dalton Trans.* **2000**, 4446. P. J. Zapf, R. P. Hammond, R. C. Haushalter, J. Zubieta, *Chem. Mater.* **1998**, *10*, 1366.

[56] A. K. Boudalis, N. Lalioti, G. A. Spyroulias, C. P. Raptopoulou, A. Terzis, V. Tangoulis, S. P. Perlepes, *J. Chem. Soc., Dalton Trans.* **2001**, 955. K. A. Abboud, C. Xu and R. S. Drago, *Acta Crystallogr. C* **1998**, *54*, 1270. K. L. Taft, A. Masschelein, S. Liu, S. J. Lippard, D. G-Shweky, A. Bino, *Inorg. Chim. Acta* **1992**, *198*, 627.

[57] A. D. Becke, *J. Chem. Phys.* **1993**, *98*, 5648.

[58] C. Lee, W. Yang, R. G. Parr, *Phys. Rev. B* **1988**, *37*, 785.

[59] B. Miehlich, A. Savin, H. Stoll, H. Preuss, *Chem. Phys. Lett.* **1989**, *157*, 200.
[60] A. J. H. Wachters, *J. Chem. Phys.* **1970**, *52*, 1033.
[61] P. J. Hay, *J. Chem. Phys.* **1977**, *66*, 4377.
[62] Gaussian 98, Revision A.11.4, M. J. Frisch, G. W. Trucks, H. B. Schlegel, G. E. Scuseria, M. A. Robb, J. R. Cheeseman, V. G. Zakrzewski, J. A. Montgomery, Jr., R. E. Stratmann, J. C. Burant, S. Dapprich, J. M. Millam, A. D. Daniels, K. N. Kudin, M. C. Strain, O. Farkas, J. Tomasi, V. Barone, M. Cossi, R. Cammi, B. Mennucci, C. Pomelli, C. Adamo, S. Clifford, J. Ochterski, G. A. Petersson, P. Y. Ayala, Q. Cui, K. Morokuma, N. Rega, P. Salvador, J. J. Dannenberg, D. K. Malick, A. D. Rabuck, K. Raghavachari, J. B. Foresman, J. Cioslowski, J. V. Ortiz, A. G. Baboul, B. B. Stefanov, G. Liu, A. Liashenko, P. Piskorz, I. Komaromi, R. Gomperts, R. L. Martin, D. J. Fox, T. Keith, M. A. Al-Laham, C. Y. Peng, A. Nanayakkara, M. Challacombe, P. M. W. Gill, B. Johnson, W. Chen, M. W. Wong, J. L. Andres, C. Gonzalez, M. Head-Gordon, E. S. Replogle, J. A. Pople, Gaussian, Inc., Pittsburgh PA, 2002.
[63] P. Gütlich, R. Link and A. X. Trautwein, Mössbauer spectroscopy and Transition Metal Chemistry. 1st edn. Springer, Berlin Heidelberg New York, 1978.
[64] P. Dufek, P. Blaha, K. Schwarz, *Phys. Rev. Lett.* **1995**, *75*, 3545.
[65] E. Krausz, *Aust. J. Chem.* **1993**, *46*, 1041.
[66] SMART, Data Collection Program for the CCD Area-Detector System; SAINT, Data Reduction and Frame Integration Program for the CCD Area-Detector System. Bruker Analytical X-ray Systems, Madison, Wisconsin, USA, 1997.
[67] G. Sheldrick, Program SADABS: Area-detector absorption correction, University of Göttingen, Germany, 1996.
[68] G. M. Sheldrick, SHELXS-97, SHELXL-97, Programs for Crystal Structure Analysis, University of Göttingen, Germany, 1997.
[69] DIAMOND 3.0b for Windows. Crystal Impact Gbr, Bonn, Germany.; **http://www.crystalimpact.com/diamond**

